ISSN NO. 2320-5407

Journal homepage: http://www.journalijar.com

INTERNATIONAL JOURNAL OF ADVANCED RESEARCH

RESEARCH ARTICLE

Optimization of microwave assisted green synthesis protocol for iron oxide nanoparticles and its application for simultaneous removal of multiple pollutants from domestic sewage

Mihir Herlekar [1]*, and Siddhivinayak Barve [1]

Department of Botany, KET's V.G. Vaze College of Arts, Science & Commerce, Mulund (E), Mumbai, (INDIA)

Manuscript Info

Manuscript History:

Received: 15 February 2015
Final Accepted: 22 March 2015
Published Online: April 2015

Key words:

Iron Oxide Nanoparticles, Green Synthesis, *Curcuma longa* L., Full Factorial, Domestic Sewage

Corresponding Author

Mihir Herlekar

Abstract

In the present study, the effect of synthesis variables on the simultaneous removal of Orthophosphate (PO_4) and Chemical Oxygen Demand (COD) from domestic sewage by iron oxide nanoparticles was evaluated by Full Factorial Experimental Design. For the first time, magnetic nanoparticles were synthesized using Turmeric (*Curcuma longa* L.) leaves (TL) as biotemplate by microwave assisted method. From the analysis of variance (ANOVA), the optimum conditions for the preparation of magnetic nanocomposite were found to be 8% plant material, 1 molar $FeCl_3$ solution and 9 hours of contact time. The metal salt concentration and contact time significantly affected PO_4 removal capacity of the nanocomposite whereas COD reduction was influenced by plant material percent and interaction effect of all three variables.

INTRODUCTION

Magnetic nanoparticles are a class of engineered nanoparticles with size less than 100 nm and which can be operated under the influence of external magnetic field (Indira and Lakshmi, 2010). Amongst these nanoparticles, nano zero-valent iron (nZVI), magnetite (Fe_3O_4) and maghemite (γ-Fe_2O_3) have emerged as a new class of important nanoparticles to be used widely in the field of environmental remediation. This is mainly due to their very efficient pollutant removal capacity, fast reaction kinetics and most importantly due to magnetism which enables its easy recovery (Tang and Lo 2013). These nanoparticles are commonly synthesized by different physical and chemical methods. Some of these conventional synthesis methods include laser pyrolysis, ball miliing, inert gas condensation, chemical vapour condensation, microemulsion, and hydrothermal synthesis. These methods have several limitations in terms of cost, low production rates and high energy requirements (Kalyanaraman et al., 1998, Roh et al., 2001, Tavakoli et al., 2007). In addition to these, magnetic nanoparticles lose their reactivity due to aggregate formation (Song and Carraway, 2005, Kim et al., 2008) and magnetism and dispersibility on air exposure (Wu et al., 2008). In addition to these limitations, conventional method for nZVI synthesis uses non polar solvents and toxic reducing agents such as sodium borohydride during synthesis (Hyeon et al., 2003). These reasons sometimes limit the environmental applications of magnetic nanoparticles. The characteristic properties of iron nanoparticles greatly depend on the synthesis procedure adopted (Margulies et al., 1996, Voogt et al., 1998). The development of clean, non toxic and environment friendly procedures for iron nanoparticle synthesis with better size control can provide a sustainable solution to this problem.

Plant-mediated synthesis of magnetic nanoparticles has remained a relatively unexplored research area with the majority of papers being published only in the last two years (Herlekar et al., 2014). In the published literature pertaining to plant extract mediated magnetic nanoparticle synthesis; very few researchers have studied the effect of the synthesis conditions on properties of as-prepared nanoparticles (Nadagouda et al., 2010, Njagi et al., 2011,

Phumying et al., 2012, Machado 2013 a, b; Ahmmad et al., 2013). Only one study has used agro waste biomass and effect of variables like type of metal salt, its concentration and contact time was optimized for size of iron nanoparticles (López-Téllez et al., 2013). All these studies have adopted univariate optimization strategies to study the effect of one variable at a time and thus underestimating the impact of interaction of variables on overall optimization process. Till now, none of the biological synthesis protocol for magnetic nanoparticle synthesis has considered multivariate system (factorial design of experiment) for estimating the effect of variables on the properties of the synthesized nanoparticles.

The problem of water pollution is getting very severe, especially in developing countries with disposal of untreated sewage. In India, only around 30% of total sewage generated gets treated (CPCB, 2009) and the discharge of untreated sewage has resulted in contamination of 75% of surface water bodies (CPHEEO, 2012). The effluents rich in organic pollutants result in the depletion of dissolved oxygen and in turn adversely affect the aquatic ecosystem (Dara, 2004). The discharge of untreated sewage with significant phosphate concentration leads to global environmental problem of eutrophication in lakes / rivers (Hua et al. 2013).

During this study, for the first time, Turmeric (*Curcuma longa* L.) leaves were used as biotemplate for iron nanoparticle synthesis. Full factorial design was used to study the importance of synthesis variables on the efficiency of plant based magnetic nanocomposite for the removal of PO_4 and COD from domestic sewage.

Materials and Methods

Materials

Turmeric (*Curcuma longa* L.) leaves were obtained from farm in Satara district in Maharashtra. The leaves were thoroughly washed with double distilled water and sun dried. These were further dried in an oven (Metalab) at 50^0 C for 48 hours, fine powdered using domestic blender and stored in air tight container and used as biotemplate (TLP).

Purified Anhydrous Iron (III) Chloride ($FeCl_3$), Concentrated Sulfuric Acid (H_2SO_4), Silver Sulfate (Ag_2SO_4), Ammonium Iron (II) Sulfate hexahydrate [$(NH_4)_2Fe(SO_4)_2.6H_2O$], Ferroin indicator were purchased from Merck India. Potassium Dichromate ($K_2Cr_2O_7$), Mercuric Sulfate ($HgSO_4$), Ammonium Molybdate, Stannous Chloride and liquor ammonia solution was obtained from Qualigens Fine Chemicals Pvt. Ltd. India. All the chemicals were of analytical grade and were used without further purification.

Full Factorial Design

Factorial designs are commonly used to obtain the best optimization of the system. One of the basic types of factorial designs used is one having two levels (2^k). In full factorial experiment, responses are measured at all combinations of the variable factor levels. This type of experiment allows simultaneous study of the effects that number of factors may have on optimization of a certain process (Montgomery, 2001, Box et al., 1978, Brasil et al., 2005) unlike univariate process in which one factor is varied at a time. Factorial design of experiments requires less number of experiments thus resulting in reduction of overall cost and time saving. These experiments determine the factors having important effects on a response as well as the effect of interaction of different group of factors.

The effect of the experimental variables [quantity of plant material (PM), metal salt concentration (MS) and contact time (CT)] on efficiency of magnetic nanocomposite for simultaneous pollutant removal was evaluated. The factor levels coded as -1 (low) and 1 (high) are given in table 1.The responses were expressed as PO_4 and COD remaining (mgL^{-1}). The results of the experimental analysis were analyzed using Minitab 16 Statistical Software to evaluate the effects, the statistical parameters and the statistical plots (normal and half normal plots of the standardized effects and Pareto chart).

Synthesis of Iron Oxide Nanoparticles

As per the design, different quantities of TLP were added to 100 ml of $FeCl_3$ solution of varying molarity and the mixture was kept on a rotary shaker at 100 rpm for specified time interval. Excess $FeCl_3$ was decanted and the plant material was microwaved for 2 minutes at 15 seconds interval. The plant material was then immersed in 5 M liquor ammonia solution for 24 hours. Excess ammonia solution was then decanted and the material was microwaved for 3 minutes at 1 minute interval. The alkali treated material was then rinsed several times with double distilled water and finally microwaved for 4 minutes at 30 seconds interval. The synthesis process was modified from Ramasahayam et al., 2012. The dried material was homogenized using mortar and pestle and used for pollutant removal experiments.

Sewage Treatability studies

Domestic sewage after grit removal was collected from Love Grove Wastewater Treatment Facility located at Worli, Mumbai, India. For initial PO_4 analysis, the sample was filtered through Whatman® Grade GF/C filter paper. Initial and final concentration of COD and PO_4 was measured by Open Reflux Method and Stannous Chloride Method respectively as per the Standard Methods for Water and Wastewater Analysis (Eaton and Franson, 2005). pH was measured using pH meter. The average concentration of PO_4 and COD in raw sewage was 1.72 mgL^{-1}, 335 mgL^{-1} respectively. Average pH value of raw sewage was 7.2.

For checking the efficiency of as prepared nanocomposites, 1 gram of each nanocomposite was added to 1 liter wastewater. The solution was mixed at 160 rpm at room temperature without any pH adjustment for 24 hours. After treatment, the nanocomposites were magnetically separated and the supernatant was filtered through Whatman® Grade GF/C filter paper and the filtrate was analyzed for PO_4 and COD. All the experiments were done in triplicates and average values are reported.

Characterization

The complete characterization was done for the nanocomposite showing the maximum PO_4 and COD removal from domestic wastewater. The preliminary characterization of nanoparticles was done using Chemito UV-Visible spectrophotometer (Model UV 2100) after recovering the embedded nanoparticles from the plant matrix. For this purpose, the nanocomposite was sonicated for 5 minutes in double distilled water and then centrifuged at 1000 rpm for 5 minutes so that TLP gets separated. The procedure was repeated thrice to ensure maximum recovery. The morphological features and elemental composition of as-synthesized nanocomposite was analyzed using SEM-EDX (FEI ESEM Quanta 200). To identify the phase of iron oxide formed, XRD analysis was performed using Shimadzu 6000 with Cu-Kα radiation source with wavelength of 0.154 nm and was operated at 40kV/30mA over 2θ range of 2 to 80^0. The scanning speed was maintained at 5^0/min. FTIR analysis of TLP and nanocomposite was done over the range of wavenumber 4000-400 cm^{-1}. The measurements were carried out on Perkin Elmer Spectrum BX FTIR spectrophotometer.

Results and Discussion

The coded values of variables along with the responses (PO_4 and COD remaining in mgL^{-1}) are illustrated in table 2. The interactions between independent variables were estimated by with the analysis of variance (ANOVA) and the main effects of pollutant remaining were identified based on the *P* value with >95% of confidence level. The main and interaction effects, coefficients of the model, standard deviation of each coefficient, regression coefficient, standard errors and T and P values for remaining PO_4 and COD concentration are shown in table 3a and table 3b respectively.

In case of remaining PO_4 concentration, metal salt concentration and contact time was significant at 5% probability level. The fit model presents an adjusted square correlation coefficient (R^2 adjusted) of 99.82%, which is very well fitting with the statistical model. Contact time and three way interaction effect of plant material, metal salt concentration and contact time significantly affected COD remaining from the domestic wastewater. In this case, R^2 adjusted was 98.49% thus fitting well with the statistical model.

Normal and half normal probability plot of the effects are used to compare the magnitude and statistical significance of main and interaction effects from a 2-level factorial design. The fitted line indicates where you would expect the points to fall if the effects were zero. Significant effects have a label and fall toward the left or right side of the graph. All the factors and interactions denoted as a circle were not significant and those shown as a square were significant.

In case of PO_4, normal plot of standardized effects showed that increase in metal salt concentration and contact time resulted in decreased concentration of PO_4 in treated sample (Fig. 1). Fig. 2 depicts normal plot of standardized effects for remaining COD concentration. The contact time and interaction effects had negative coefficients and with increase in these values, lesser COD was left over in the treated sample.

The half normal plot displays the absolute value of all effects, positive and negative. Instead of putting negative effects to the left and positive effects to the right, all the significant effects are on the right side of the origin for comparing their relative magnitudes. For remaining PO_4 concentration, absolute standardized effect of metal salt concentration was more significant than that of the contact time as can be seen from Fig. 3. Contact time affected COD removal more than the three-way interaction effect (Fig. 4).

ANOVA is a statistical method that divides total variation into its component parts and each component is associated with a different source of variation. The interaction effects are estimated and analyzed using ANOVA. Table 4 shows ANOVA results for full factorial design with two centre points for remaining PO_4 and COD concentration. The sum of squares used to determine the effect of factors, Fischer's *F* ratios and *P* values were also estimated. In addition, the analysis of variance showed that this model did not present curvature for both the pollutant removal as the probability was 0.268 and 0.115 for remaining PO_4 and COD concentration respectively.

The relative importance of the individual and interaction effects was highlighted by Pareto chart of the standardized effects. In order to identify whether the calculated effects were significantly different from zero, Student's *t*-test was performed and horizontal columns in Pareto chart showed these values for each effect. For a 95% confidence level and nine degrees of freedom *t* value was equal to 12.71. The minimum statistically significant effect magnitude for 95% confidence level is represented by the vertical line in the chart. Two values (metal salt concentration and contact time) higher than 12.71 ($P = 0.05$) were located on the right side of the dash line and were considered to be significant for the removal of phosphate from the sample (Fig. 5). As depicted in Fig. 6, in case of the remaining COD concentration, contact time and three-way interaction effect was found to have value more than 12.71.

The maximum iron content (data not shown) was observed in material number 2 generated through factorial design. This nanocomposite showed highest PO_4 removal (83%). The reason for high efficiency of this nanocomposite in PO_4 removal is due to its ability to form monodentate inner sphere complex with phosphorus at around neutral pH (Sarkar et al., 2008) which holds true for sewage. Highly efficient phosphorus adsorbing magnetic nanocomposites have been previously synthesized for phosphate removal from synthetic samples (Ramasahayam et al., 2012, Viswanathan 2013). In comparison, 32% of initial PO_4 concentration could be removed in case of alkali treated and microwaved plant material without embedded nanoparticles. COD reduction of 44% was achieved using plant material treated with alkali and subsequent microwaving whereas magnetic nanocomposite removed 83% of COD from domestic sewage sample. The amount of iron/iron oxide incorporated into in the composite played an important role in organic matter removal (Ramasahayam et al., 2012).

Table 1: Coded Levels of Factor

Factors	**Levels**		
	-	**0**	**+**
PM (%)	4	6	8
MS (Molar)	0.01	0.505	1
CT (Hours)	3	6	9

Table 2: Optimization of PO_4 and COD Remaining

Experiment	**PM**	**MS**	**CT**	**Remaining Concentration (mgL^{-1})**	
				PO_4	**COD**
1	6	0.505	6	0.77	70
2	8	1	9	**0.35**	**58**
3	6	0.505	6	0.79	68
4	8	1	3	0.59	88
5	4	1	9	0.46	64
6	8	0.01	3	1.33	90
7	8	0.01	9	0.95	76
8	4	0.01	3	1.23	96
9	4	0.01	9	1.05	68
10	4	1	3	0.48	70

Table 3a: Factorial Fit: PO_4 Remaining (mgL^{-1}) versus PM, MS and CT

Term	Effect	Coefficient	SE of coefficient	*P*
Main Factors		0.8050	0.005000	0.004
PM	- 0.1050	- 0.0525	0.005000	0.060
MS	- 0.6700	- 0.3350	0.005000	0.010
CT	- 0.2050	- 0.1025	0.005000	0.031
Interaction of two factors				
PM.MS	- 0.0050	- 0.0025	0.005000	0.705
PM.CT	0.0000	0.0000	0.005000	1.000
MS.CT	0.0750	0.0375	0.005000	0.084
Interaction of three factors				
PM.MS.CT	0.0000	0.0000	0.005000	1.000
Central point (CP)		- 0.0250	0.011180	0.268
S = 0.0141421	R^2 = 99.98%		R^2 (adj)= 99.82%	

Table 3b: Factorial Fit: COD Remaining (mgL^{-1}) versus PM, MS and CT

Term	Effect	Coefficient	SE of coefficient	*P*
Main Factors		75.125	0.5000	0.004
PM	- 0.250	- 0.125	0.5000	0.844
MS	- 7.750	- 3.875	0.5000	0.082
CT	- 17.250	- 8.625	0.5000	0.037
Interaction of two factors				
PM.MS	5.750	2.875	0.5000	0.110
PM.CT	1.250	0.625	0.5000	0.430
MS.CT	- 3.250	- 1.625	0.5000	0.190
Interaction of three factors				
PM.MS.CT	- 12.750	- 6.375	0.5000	0.050
Central point (CP)		- 6.125	1.1180	0.115
S = 1.41421	R^2 = 99.83%		R^2(adj) = 98.49%	

Table 4: Analysis of Variance for mgL^{-1} of PO_4 and COD Remaining for Full 2^3 Factorial Design

Source	DF	Seq SS	Adj SS	Adj MS	*F*	*P*
PO_4 remaining						
Main effects	3	1.00390	1.00390	0.334633	1673.17	0.018
Two-way interactions	3	0.01130	0.01130	0.003767	18.83	0.167
Three-way interactions	1	0.00000	0.00000	0.000000		
Curvature	1	0.00100	0.00100	0.001000	5.00	0.268
Residual error	1	0.00020	0.00020	0.000200		
Pure error	1	0.00020	0.00020	0.000200		
Total	9	1.01640				
COD remaining						
Main effects	3	715.37	715.375	238.458	119.23	0.067
Two-way interactions	3	90.38	90.375	30.125	15.06	0.187
Three-way interactions	1	325.12	325.125	325.125	162.56	0.050
Curvature	1	60.02	60.025	60.025	30.01	0.115
Residual error	1	2	2	2		
Pure error	1	2	2	2		
Total	9	1192.00				

DF- degree of freedom, Seq SS- sequential sum of squares, Adj SS- adjusted sum of squares, *F*- Factor F, *P*- Probability

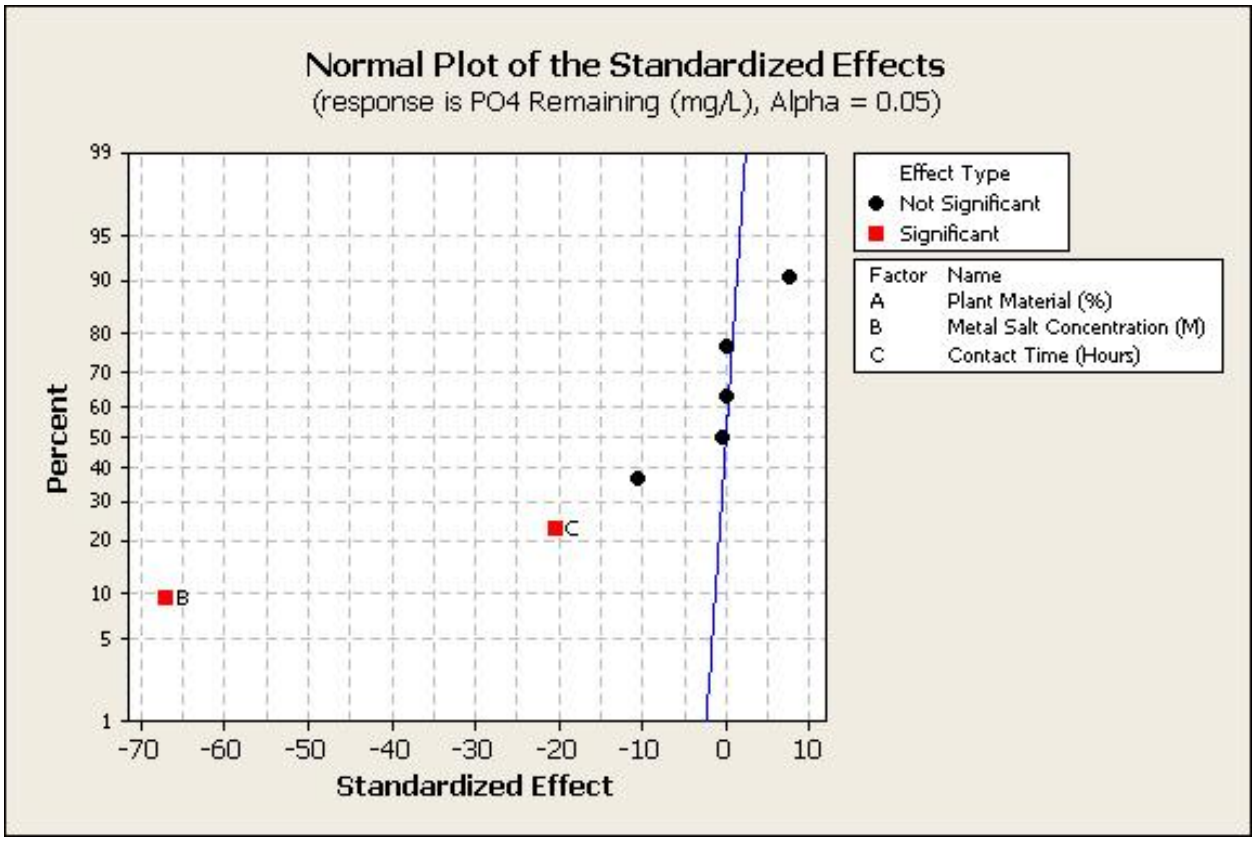

Fig.1 : Normal Plot of Standardized Effects for Remaining Phosphate Concentrations

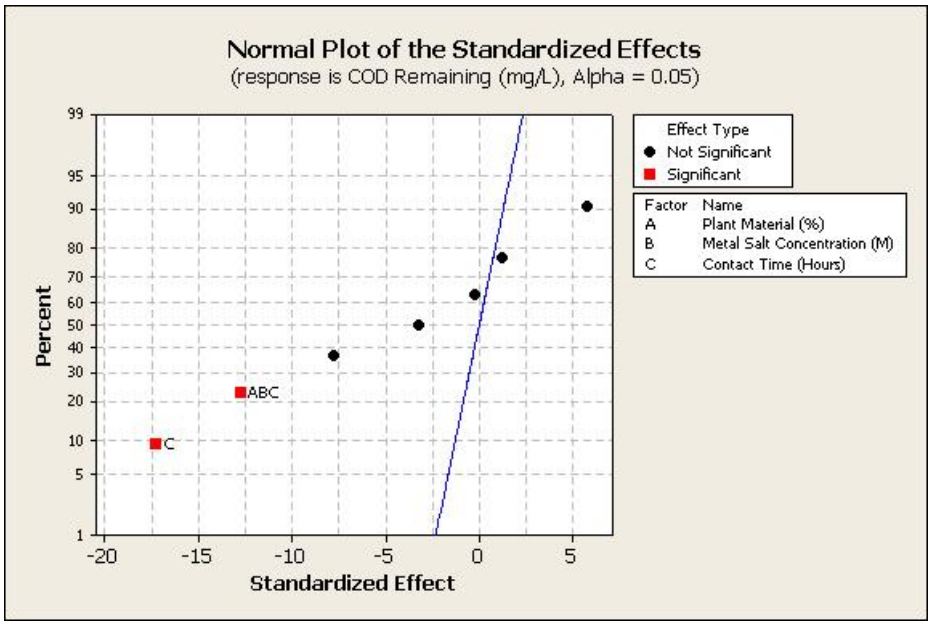

Fig. 2 : Normal Plot of Standardized Effects for Remaining COD Concentrations

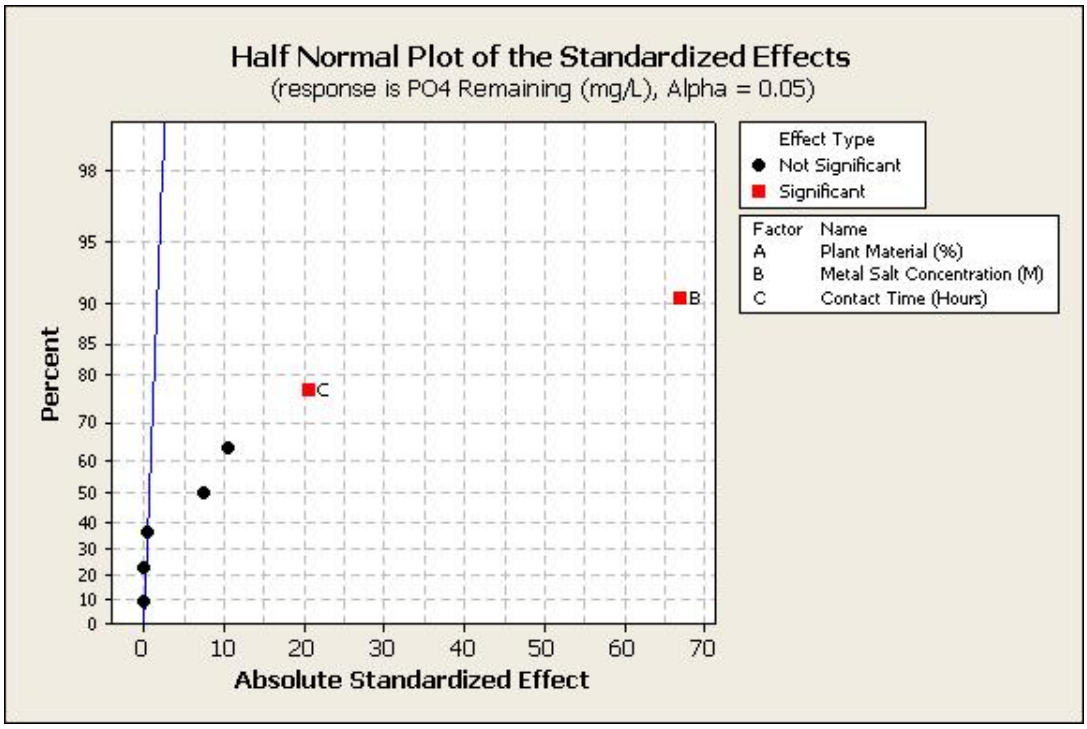

Fig. 3 : Half Normal Plot of Standardized Effects for Remaining PO_4 Concentrations

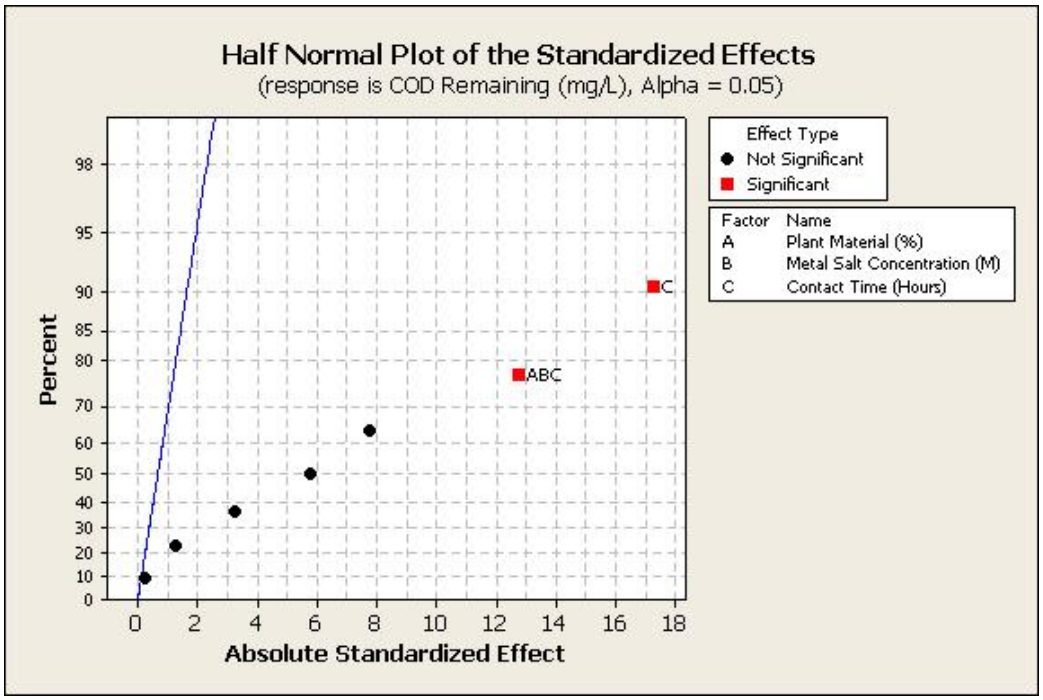

Fig. 4 : Half Normal Plot of Standardized Effects for Remaining COD Concentrations

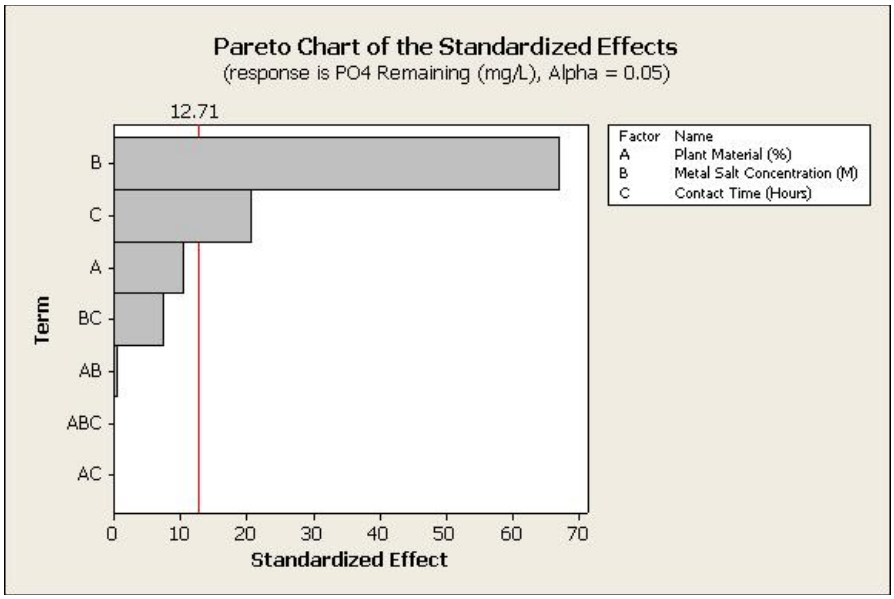

Fig. 5 : Pareto Chart for Remaining PO_4 Concentrations

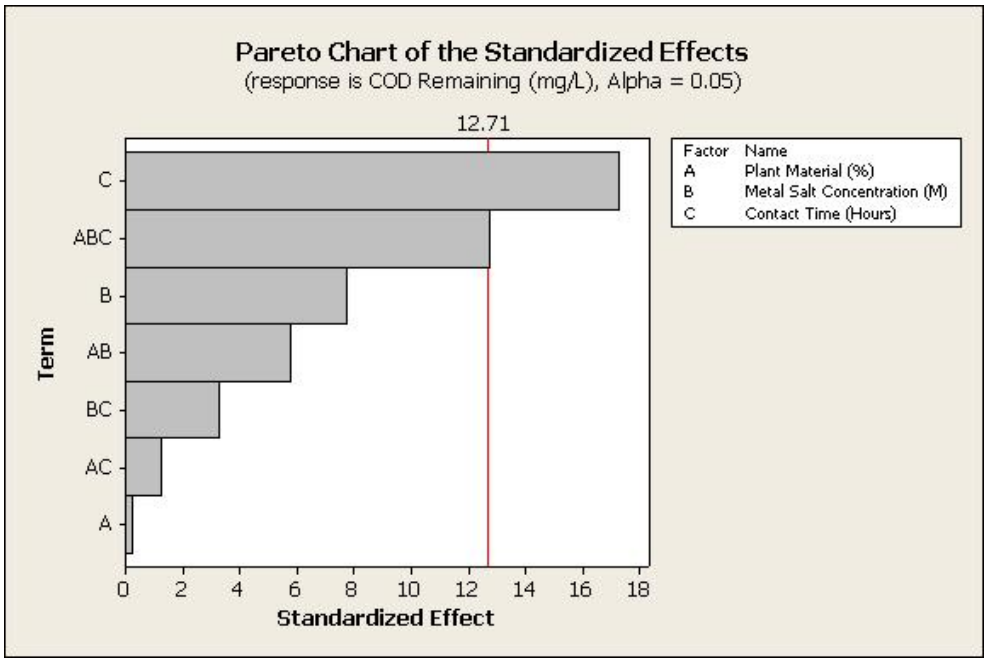

Fig. 6 : Pareto Chart for Remaining COD Concentrations

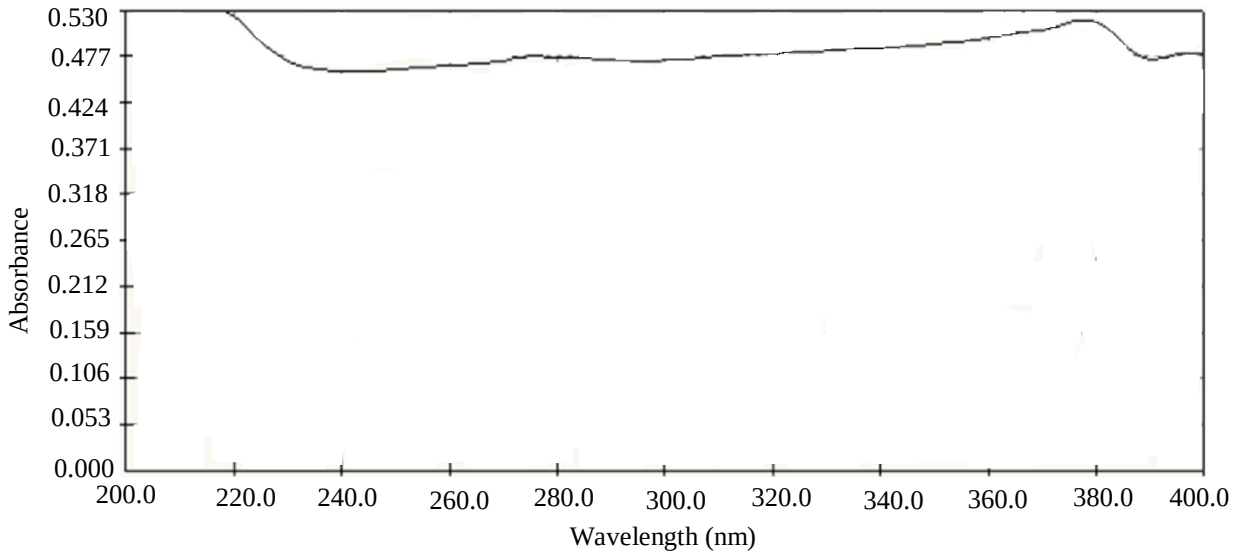

Fig. 7 : UV-visible Absorption Spectra of Iron Nanoparticles

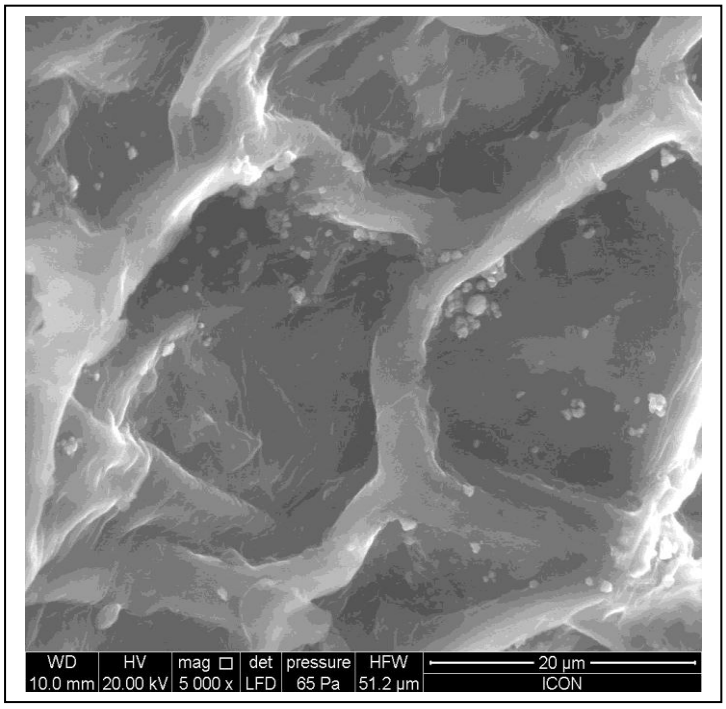

Fig. 8: SEM Image of Iron Oxide Nanoparticles

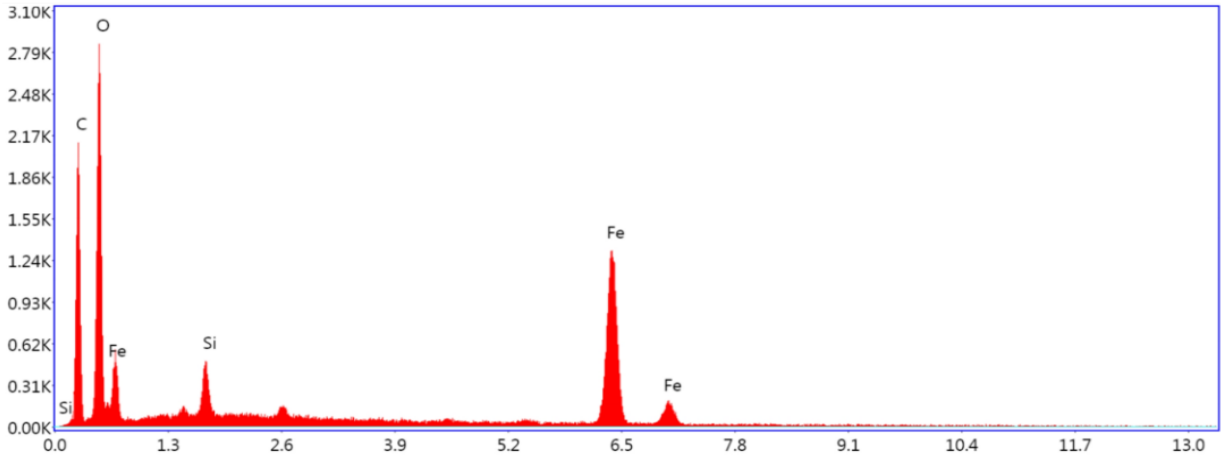

Fig. 9: Elemental Composition pf Iron Oxide Nanoparticles

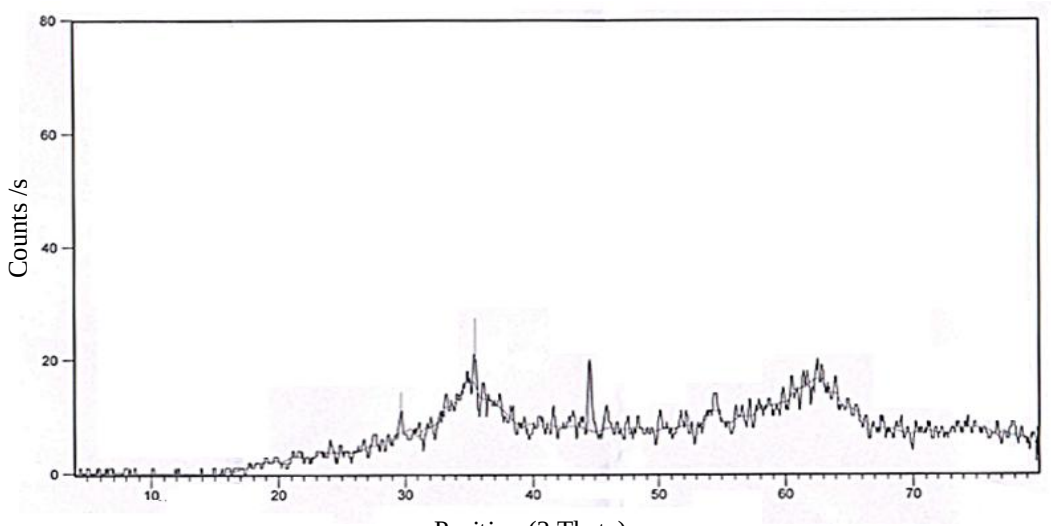

Fig. 10 : XRD Pattern of Iron Nanoparticles

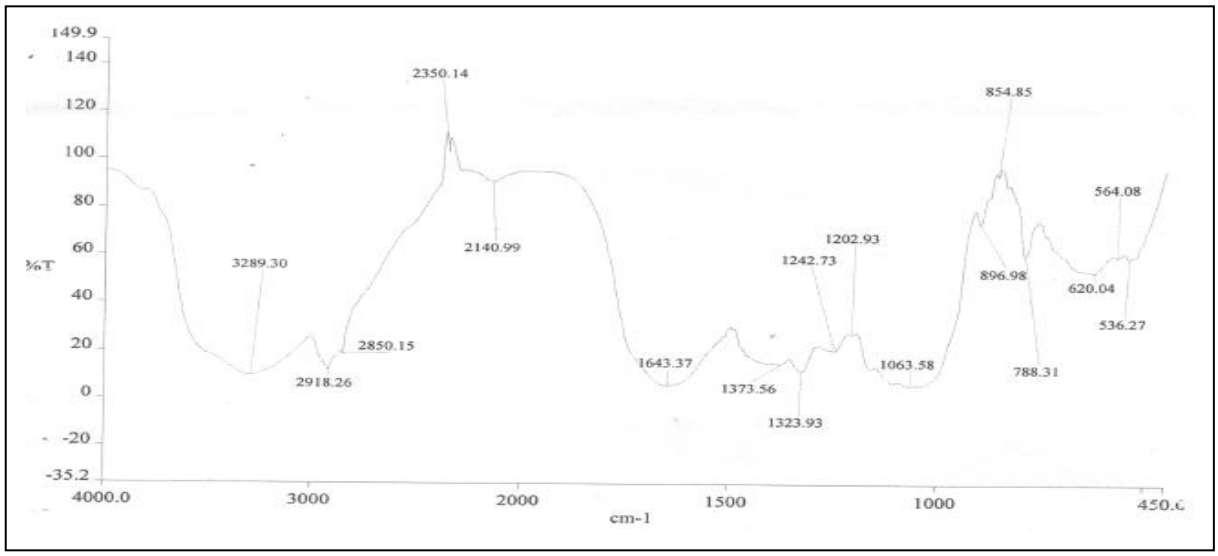

Fig.11a: FTIR Measurements of TLP

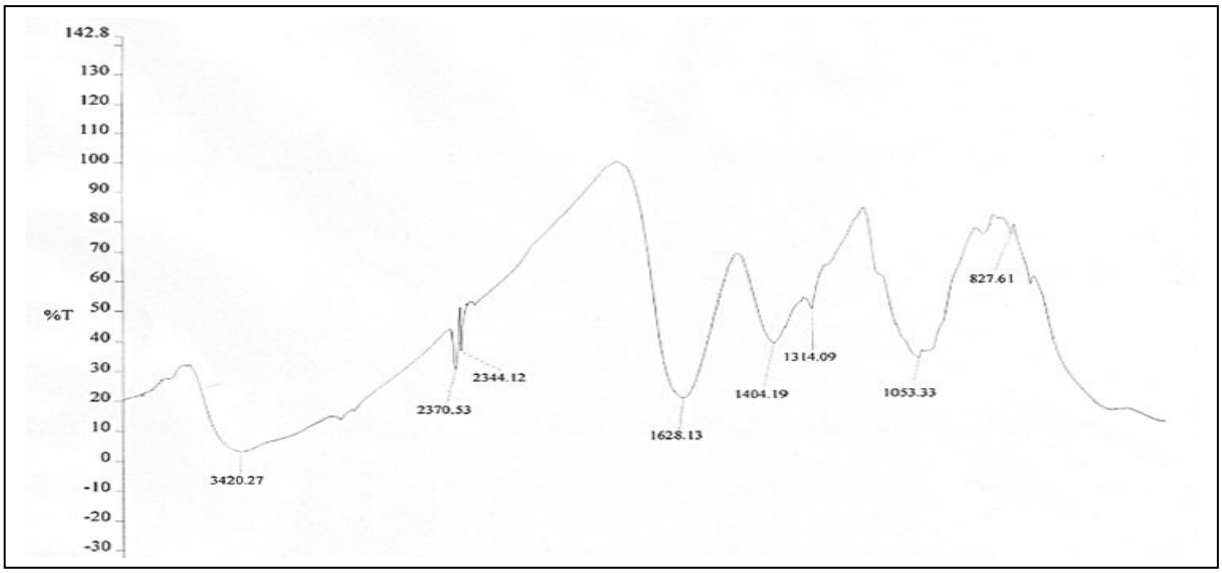

Fig. 11b: FTIR Measurements of Nanocomposite

Characterization

The preliminary characterization of synthesized nanoparticles by UV-Visible Spectroscopy has proven to be very useful technique for the analysis of nanoparticles (Sastry et al., 1998). The UV- Vis spectra of supernatant solution containing nanoparticles were taken against the spectra of double distilled water as blank. The UV-visible spectra were recorded over the 200-400 nm range. As depicted in Fig. 7, Iron nanoparticles showed characteristic peak of magnetite at 377 nm as previously described by Behera et al., 2012.

SEM images of iron oxide nanoparticles are shown in Fig. 8. The nanoparticles synthesized using TLP were spherical in shape and were found to be evenly dispersed in the plant matrix.

The elemental composition of Fe NPs was studied using EDS. As can be seen from the Fig. 9, the predominant peaks were of iron (Fe), Oxygen (O) and Carbon (C). The signals for C and O were mainly due to the different phytochemicals present in plant powder. The signal for oxygen also confirms the fact that iron oxide nanoparticles have been synthesized. The weight percent (wt %) of nanoparticles was measured to be 25.52% for Fe, 35.99% for O and 36.98% for C. The high Fe loading enables easy magnetic recovery of as-prepared nanoparticles. Some minor loading from silica (Si) was also observed. It would be arising from the plant material. As cited from relevant

literature, the iron content of Fe NPs synthesized during the study is found to be comparable with iron nanoparticles obtained from other plant materials.

XRD patterns obtained for nanocomposite is shown in Fig. 10. The diffraction peaks were observed at 2θ values of 29.67, 35.47 and 44.52. The peaks at 29.67 and 35.47 can be indexed to the formation of magnetite (Senthil et al., 2012, Kumar et al., 2013). The peak at 44.52 corresponds to zero valent iron nanoparticles (Ramasahayam et al., 2012, Kuang et al., 2013).

The crystallite size of TL – Fe NPs was estimated using the Debye-Scherrer equation, which gives a relationship between peak broadening in XRD and particle size that is demonstrated by following equation:

$$d = k\lambda / (\beta \bullet \cos\theta)$$

where, d is the particle size of the crystal, k is Scherrer constant, λ is the X-ray wavelength (0.154 nm), β is the width of the XRD peak at half-height, and θ is the Bragg diffraction angle. Using the Scherrer equation, the average crystallite sizes of the magnetic Fe_3O_4-NPs are found to be in the range of 17.9 to 28.7 nm. The size of nZVI was calculated to be 23.8 nm.

FTIR measurements of TLP and nanoparticles (Fig. 11a and 11b) were carried out to understand the involvement of biomolecules present in turmeric leaves powder in nanoparticle synthesis. Turmeric leaves have high polyphenol content (Yan and Asmah, 2010, Arutselvi et al., 2012) and many authors have highlighted its role in forming complex with metal ions and reduce the metals (Tandon et al., 2013, Venkateswarlu et al., 2013, Wang et al., 2014). Involvement of polyphenols and aldehydes in turmeric leaves in magnetite nanoparticle synthesis is highlighted by the shift of peak to 3420.37 cm^{-1} and 1628.13 cm^{-1} respectively in microwaved material. As mentioned by Ramasahayam et al., 2012, alkali treatment and further microwaving has resulted the formation of reduced iron nanoparticles. Iron oxide peaks are characterized by strong bands in low wavelength region of 1000-400 cm^{-1}. The peak at 827.61 cm^{-1} indicates Fe-OH vibration (Sangeetha and Kumaraguru, 2015).

The detailed studies are being carried out to optimize the pollutant removal (especially in case of phosphate so as to avoid eutrophication) of this novel nanoadsorbent. The reaction kinetics and adsorption mechanism for removal of pollutants is also being studied. Also, the stability and reusability of nanocomposite is being tested.

Conclusion

Turmeric leaves were used as biotemplate to synthesize magnetically recoverable bionanocomposite with multiple pollutant removal capacity. In this study, for the first time, multivariate system (factorial design of experiment) was applied for estimating the effect of variables on the properties of the biologically synthesized nanoparticles. Contact time between metal salt solution and plant material is the most influential factor determining PO_4 and COD removal. The optimum conditions for the synthesis of nanocomposite using full factorial design were found to be 8% plant material, 1 molar $FeCl_3$ solution and 9 hours contact time. These optimum conditions resulted in maximum PO_4 (82%) and COD (83%) removal. The experimental results showed applicability of nanocomposite as a novel option for sewage treatment.

Acknowledgement

Authors gratefully acknowledge the technical support from the KET's V. G. Vaze College and CSIR-NEERI, Mumbai Zonal Laboratory.

References

Ahmmad, B., Leonard, K., Islam, Md. S., Kurawaki, J., Muruganandham, M., Ohkubo, T., Kuroda, Y., (2013). Green synthesis of mesoporous hematite (α-Fe_2O_3) nanoparticles and their photocatalytic activity. Adv. Powder Technol. 24(1): 160–167.

Arutselvi, R., Balasaravanan, T., Ponmurugan, P., Muthu Saranji, N., Suresh P. (2012). Phytochemical Screening and Comparative Study of Anti Microbial Activity of Leaves and Rhizomes of Turmeric Varieties. Asian J. Plant Sci. Res. 2(2): 212-219.

Behera, S.S., Patra, J.K., Pramanik, K., Panda, N., Thatoi, H. (2012). Characterization and Evaluation of Antibacterial Activities of Chemically Synthesized Iron Oxide Nanoparticles, World J. Nano Sci. Eng. 2(4): 196-200.

Box, G.E.P., Hunter, W.G., Hunter, J.S. (1978). Statistics for experimenters- an introduction to design, data analysis and model building. New York: John Wiley & Sons

Brasil, J.L., Martins, L.C., Ev, R.R., Dupont, J., Dias, S.L.P., Sales, J.A.A. (2005). Factorial design for optimization of flow-injection preconcentration procedure for copper (II) determination in natural waters, using 2-amino-methylpyridine grafted silica gel as adsorbent and spectroscopic detection (2005). Int. J. Env. Anal. Chem. 15: 475-491.

Central Pollution Control Board (2009). Status of water supply, wastewater generation and treatment in class- I cities & class- II towns of India. Series: CUPS/70/2009-10.
http://www.cpcb.nic.in/upload/NewItems/NewItem_153_Foreword.pdf. Accessed 27 July 2011

Central Public Health and Environmental Engineering Organization (2012). Part A: Engineering. CPHEEO, Ministry of Urban Development, Government of India.
http://cpheeo.nic.in/WriteReadData/Cpheeo_Sewarage_Latest/PartA-HighResolution/Chapter% 201.pdf. Accessed 10 October 2013

Eaton, A., Franson, M. (Eds.) (2005). Standard Methods for the Examination of Water and Wastewater. USA: American Public Health Association.

Herlekar, M., Barve, S., Kumar, R. (2014). Plant-Mediated Green Synthesis of Iron Nanoparticles. J. Nanoparticles, Article ID 140614, 9 pages.

Hua M, Xiao L, Pan B, Zhang Q (2013). Validation of polymer-based nano-iron oxide in further phosphorus removal from bioeffluent: laboratory and scaled-up study. Front. Environ. Sci. Eng. 7(3): 435-441

Hyeon, T. (2003). Chemical synthesis of magnetic nanoparticles. Chem. Commun. 9: 927-934.

Indira, T.K., and Lakshmi, P.K. (2010). Magnetic Nanoparticles – A review. Int. J. Pharma. Sci. Nanotechnol. 3(3): 1035-1042.

Kalyanaraman, R., Yoo, S., Krupashankara, M.S., Sudarshan, T.S., Dowding, R.J. (1998). Synthesis and consolidation of iron nanopowders. Nanostruct. Mater. 10(8): 1379–1392.

Kim, J. H., Tratnyek, P. G., Chang, Y. S. (2008). Rapid Dechlorination of Polychlorinated Dibenzo-p-dioxins by Bimetallic and Nanosized Zerovalent Iron. Environ. Sci. Technol. 42: 4106–4112.

Kuang, Y., Wang, Q., Chen, Z., Megharaj, M., Naidu, R. (2013). Heterogeneous Fenton-like oxidation of monochlorobenzene using green synthesis of iron nanoparticles," J Colloid Interface Sci. 410: 67–73.

Kumar, K. M., Mandal, B. K., Kumar, K. S., Reddy, P. S., Sreedhar, B. (2013). Biobased green method to synthesize palladium and iron nanoparticles using *Terminalia chebula* aqueous extract. Spectrochimica Acta Part A: Mol. Biomol. Spectro. 102: 128–133.

López-Téllez, G., Balderas-Hern´andez, P., Barrera-D´ıaz, C. E., Vilchis-Nestor, A. R., Roa-Morales, G., Bilyeu, B. (2013). Green method to form iron oxide nanorods in orange peels for chromium (VI) reduction. J. Nanosci. Nanotechnol. 13(3): 2354–2361.

Machado, S., Pinto, S. L., Grosso, J. P., Nouws, H. P. A., Albergaria, J. T., Delerue-Matos, C. (2013 a). Green production of zerovalent iron nanoparticles using tree leaf extracts. Sci. Tot. Env. 445-446: 1–8.

Machado, S., Stawiński, W., Slonina, P. Pinto, A.R., Grosso, J.P., Nouws, H.P.A., Albergaria, J.T., Delerue-Matos, C. (2013b). Application of green zero-valent iron nanoparticles to the remediation of soils contaminated with ibuprofen. Sci. Tot. Env. 461-462: 323–329.

Margulies, D.T., Parker, F.T., Spada, F.E., Goldman, R.S., Sinclair, J., Li, R., Berkowitz, A.E., (1996). Anomalous moment and anisotropy behavior in Fe_3O_4 films. Phys. Rev. B. 53: 9175-9187.

Montogmery, D.C., (2001). Design and analysis of experiments. 5th edition New York: John Wiley & Sons

Nadagouda, M. N., Castle, A. B., Murdock, R. C., Hussain, S. M. and Varma, R. S. (2010). In vitro biocompatibility of nanoscale zerovalent iron particles (NZVI) synthesized using tea polyphenols. Green Chem. 12(1): 114–122.

Njagi, E.C., Huang, H. Stafford, L. Genuino, **H., Galindo, H.M., Collins, J.B., Hoag, G.E., and Suib, S.L. (2011)**. Biosynthesis of iron and silver nanoparticles at room temperature using aqueous sorghum bran extracts. Langmuir 27(1): 264–271.

Phumying, S., Labuayai, S., Thomas, C., Amornkitbamrung, V., Swatsitang, E., Maensiri, S. (2013). Aloe vera plant-extracted solution hydrothermal synthesis and magnetic properties of magnetite (Fe_3O_4) nanoparticles. Applied Physics A 111(4): 1187–1193.

Ramasahayam, S., Gunawan, G., Finlay, C., Viswanathan, T. (2012). Renewable Resource-Based Magnetic Nanocomposites for Removal and Recovery of Phosphorous from Contaminated Waters. Water Air Soil Poll. 223: 4853-4863.

Roh, Y., Lauf, R.J., McMillan, A.D., Zhang, C., Rawn, C.J., Bai, J., Phelps, T.J. (2001). Microbial synthesis and the characterization of metal-substituted magnetites. Solid State Commun. 118 (10): 529-534.

Sangeetha, N. and Kumaraguru, A.K. (2015). Antitumor Effects and Characterization of Biosynthesized Iron Oxide Nanoparticles Using Seaweeds of Gulf of Mannar. Int. J. Pharm. Pharma. Sci. 7(2): 469-476

Sarkar, S., Blaney, L.M., Gupta, A., Ghosh, D., Sengupta, A.K. (2008). Arsenic Removal from Groundwater and Its Safe Containment in a Rural Environment: Validation of a Sustainable Approach. Environ. Sci. Technol. 42: 4268-4273.

Sastry, M., Patil, V., Sainkar, S. R. (1998). Electrostatically Controlled Diffusion of Carboxylic Acid Derivatized Silver Colloidal Particles in Thermally Evaporated Fatty Amine Films. J. Phys. Chem. B, 102: 1404–1410.

Senthil, M., and Ramesh, C. (2012). Biogenic synthesis of Fe_3O_4 nanoparticles using Tridax procumbens leaf extract and its antibacterial activity on *Pseudomonas aeruginosa*. Digest J. Nanomater. Biostruct. 7(4): 1655–1661.

Song, H., and Carraway, E. R. (2005). Reduction of Chlorinated Ethanes by Nanosized Zero-Valent Iron: Kinetics, Pathways, and Effects of Reaction Conditions. Environ. Sci. Technol. 39: 6237–6245.

Tandon, P., Shukla, R., Singh, S. (2013). Removal of Arsenic (III) from Water with Clay-Supported Zerovalent Iron Nanoparticles Synthesized with the Help of Tea Liquor, Ind. Eng. Chem. Res. 52(30): 10052-10058.

Tang, S.C., and Lo, I. M. (2013). Magnetic nanoparticles: essential factors for sustainable environmental applications. Water Res. 47: 2613-2632.

Tavakoli, A., Sohrabi, M. and Kargari, A. (2007). A review of methods for synthesis of nanostructured metals with emphasis on iron compounds. Chem. Pap. 61(3): 151–170.

Venkateswarlu, S., Subba Rao, Y., Balaji, T., Prathima, B., Jyothi, N.V.V. (2013). Biogenic Synthesis of Fe_3O_4 Magnetic Nanoparticles using Plantain Peel Extract. Materials Lett. 100: 241-244.

Viswanathan T. (2013). Renewable Resource-based Metal Oxide-containing Materials and Applications of the Same. U.S. Patent 0233802 A1.

Voogt, F.C., Palstra, T.T.M., Niesen, L., Rogojamu, O.C., James, M.A., Hmiba, T. (1998). Superparamagnetic behavior of structural domains in epitaxial ultrathin magnetite films. Phys. Rev. B. 57: R8107-R8110.

Wang, T., Jin, X., Chen, Z., Megharaj, M., Naidu, R. (2014). Green Synthesis of Fe Nanoparticles using Eucalyptus Leaf Extracts for Treatment of Eutrophic Wastewater. Sci. Total Environ. 466-467: 210-213.

Wu, W., He, Q., Jiang, C. (2008). Magnetic iron oxide nanoparticles: synthesis and surface functionalization strategies. Nanoscale Res. Lett. 3: 397-415.

Yan, S.W., and Asmah, R. (2010). Comparison of Total Phenolic Contents and Antioxidant Activities of Turmeric Leaf, Pandan Leaf and Torch Ginger Flower. J. Int. Food Res. 17: 417-423.